Combining marker-based cell classification and super-resolution imaging on Aplo Scope

SUMMARY

One of the main challenges for SMLM is to inform how nanoscale behavior varies on a cell-by-cell basis within heterogeneous cell populations. ONI's Aplo Scope and its integrated software solution, CODI, offer a versatile platform to classify cells into subpopulations according to their marker expression. Combining diffraction-limited multi-marker imaging with Single-Molecule Localization Microscopy (SMLM) enables reporting of the nanoscale organization of signaling proteins within each subpopulation with exceptional sensitivity and precision.

Aplo Scope enables:

- Detection and relative quantification of multiple cell population markers
- Classification of heterogeneous samples into discrete subpopulations
- Visualization of surface protein organization with 20 nm resolution
- Comparison of the informative nanoscale behavior across multiple subpopulations

INTRODUCTION

The ability to characterize the nanoscale behavior of molecules has been used to significantly advance understanding in a wide range of biomedical fields, including oncology, immunology, and neurobiology[1-3]. The diffraction limit of light restricts the resolution of conventional microscopes to ~200 nm and has long been considered an impassable barrier, making nanoscale information inaccessible. It has only been with the emergence of super-resolution methods such as single-molecule localization microscopy (SMLM)[4] that it has been possible to overcome this limitation. SMLM encompasses a family of related techniques that use the on-off blinking of fluorophores to temporally separate signals from individual molecules. dSTORM (direct Stochastic Optical Reconstruction Microscopy[5]), the most frequently used SMLM method, achieves blinking through the stochastic activation and deactivation of specific fluorophores at high laser powers, and is able to localize molecules individually with sub-20 nm precision.

Connecting nanoscale features to population-level functional differences is essential to fully understand a wide range of complex biological systems given the large heterogeneity found in cell differentiation, function, health, and activation status[6-8] . As an example, T cells exhibit extreme cell-to-cell heterogeneity due to the large number of different T cell subpopulations, each with distinct functions and responses to stimuli. These subpopulations are well characterized according to the expression of relevant surface markers, transcription factors, or secreted cytokines[9] , due in large part to extensive use of flow cytometry methods by the field. With an appropriate instrument setup, it is possible to perform microscopy-based cell classification following staining for markers of interest.

CHALLENGES

Historically, it has not been possible to obtain super-resolved information within the context of multi-marker cell classification. Flow cytometry[10] has proved powerful for simultaneously high-number marker detection, but it is not SMLM-compatible. Single-cell RNA sequencing[11] or antibody-barcoding proteomics[12] can provide whole transcriptome or proteome read depths, but sample preparation requirements destroy nanoscale features. Imaging cytometry, which uses widefield microscopy instead of a flow column[13], has matched some of the breadth and speed of flow cytometry, yet it is unable to deliver the complex optical requirements for SMLM. Similarly, SMLM microscopes have not provided the channel breadth or field size needed for imaging cytometry, with higher-level cell classification often performed independently from super-resolved nanoscale information, or sequentially using cell isolation or sorting.

Aplo Scope represents the next generation of super-resolution microscopes, seamlessly combining diffraction-limited with high-performance SMLM, and allowing robust multi-marker imaging in the same sample. Its unique architecture of 4 laser lines and 10 independent filters allow multiple combinations to discriminate a wide range of fluorophores and increase the number of channels used for marker-based cell classification, leaving additional channels for parallel SMLM. Alongside the large 110 x 110 µm field-of-view and user-friendly software, this makes Aplo Scope a potent tool for classifying large numbers of cells and interrogating their nanoscale behavior. Here, 5-channel cell classification and 2-channel SMLM was combined in the context of activated T cells, exemplifying the utility and fidelity of the method.

METHODS

Primary human T cells were isolated from a single donor and placed into cell culture for 48 h with 50 U/mL IL-2, then a further 24 h without IL-2. Artificial supported lipid bilayers (SLBs) were prepared by depositing micelles of 87.5% DOPC, 12.5% DGS-NTA(Ni) onto plasma-etched glass coverslips within 6-lane imaging chambers. SLBs were blocked, washed, and incubated with recombinant His-tagged proteins of interest: anti-CD3-Fab (30 molecules/µm^2), ICAM1 (200 molecules/µm^2), and PDL1 (20 molecules/µm^2). The specific combination of unconjugated proteins or conjugated to different dyes varied for each sample. Equivalent lanes were coated with 0.01% poly-L-lysine (PLL) for 30 min then washed with ultrapure water. ~5 × 10^5 primary T cells were added to each SLB or PLL lane in OptiMEM and incubated at 37°C for 7 min, then fixed using the ONI Discovery Kit™: dSTORM in cells fixative B, paraformaldehyde (PFA) supplemented with glutaraldehyde for strong fixation. Cells were washed, quenched, permeabilized, and blocked using the Discovery Kit. Targets were probed using primary antibodies: anti-CD4 (SK3)-eFluor450, anti-CD25 (B-B10)-CF®405L, anti-CD8 (YCT.182.20)-Alexa Fluor™ 488, anti-FoxP3 (3G3)-DyLight™-515LS, anti-PD1 (EH12.2H7)-CF®700, anti-TCR (IP26)-AZDye 647, and unconjugated anti-pZAP70 (2704). Staining was performed at 4°C overnight, followed by washing and incubation for 2 h at room temperature with secondary F(ab')2 conjugated to CF®583R. Cells were all thoroughly washed after staining and post-fixed with PFA, then mounted in ONI's BCubed imaging buffer.

Images were collected on an ONI Aplo Scope and analyzed using CODI. For diffraction-limited imaging, 5 frames for 250 ms were acquired and averaged into a single image. Channel intensity values were derived by isolating an individual region of interest corresponding to each cell, and deriving the mean gray value per channel. Compensation was performed between relevant channels by reference to single-color standards to determine any bleedthrough, and applied as a pixel-by-pixel correction in each channel, all using Image J. For dSTORM, 3000 frames of 30 ms were collected for each of the AZ647 and CF583R channels. Localization analysis was performed on CODI, filtering and clustering the TCR channel using the DBSCAN algorithm with a 75 nm set length scale ($\boldsymbol{\varepsilon}$). The CODI counting tool was used to report pZAP70 localizations within a 100 nm diameter of each TCR cluster. For flow cytometry, cells were fixed, quenched, permeabilized, and blocked as above, and stained with the same primary antibody panel without anti-TCR and anti-pZAP70. Data was collected on a BD LSRFortessa™ X-20.

RESULTS

Primary human T cells were immobilized on a PLL-coated imaging surface, stained, and imaged using ONI's Aplo Scope to exemplify how nanoscale information can be obtained within an informed context of cell identity. The versatility of Aplo Scope's laser-filter combinations allowed five T cell population markers (CD4, CD25, CD8, FoxP3, and PD1) to be simultaneously distinguished with high specificity and minimal cross-talk when using antibodies directly-conjugated with eFluor450, CF®405L, Alexa Fluor™ 488, DyLight™-515LS, and CF®700 (Figure 1A). The presence, absence, and relative abundance of each marker was quantified, allowing a marker profile to be assigned to each cell. In total, 15 fields of 110 x 110 µm were acquired, totalling 326 cells. The combination used allowed eight distinct subpopulations to be identified with confidence. Firstly, cells were gated into either the $CD4^+$ helper T cell population or $CD8^+$ cytotoxic T cell population, with a small fraction of CD4/8 double-positive or double-negative cells. These two roughly equally-sized populations were then subdivided into $PD1^-CD25^-$ (resting cells), $PD1^{=/low}CD25^+$ (activated cells), $PD1^{++}$ (exhausted cells), or $FoxP3^+$ (regulatory cells) (Figures 1B and 1C). $PD1^{low}CD25^-$ cells were gated but not defined as they represent an ambiguous population. In all cases, positivity thresholds were defined based on equivalent data taken with relevant isotype control staining.

The overall distribution of T cell populations was consistent with that expected of a healthy donor: a majority of resting cells (which can represent both naïve and memory cells), a smaller subset of activated cells, and only small populations of exhausted or regulatory cells. The same cell sample stained with the same antibody panel was analysed on a flow cytometer, with the imaging-derived data broadly agreeing with the flow data (Figure 1D). Minor differences in absolute percentages between the two methods were most likely due to the cell count difference (326 for imaging vs 5000 for flow cytometry) and the increased laser power of Aplo Scope compared to the LSRFortessa X-20 cytometer. The population composition was consistent between the two methods, including for example, the fact that the small $FoxP3^+$ regulatory subpopulation only exists in the $CD4^+$ population (6.0% for imaging, 1.4% for flow) and not in the $CD8^+$ population (0.6% for imaging, 0.0% for flow).

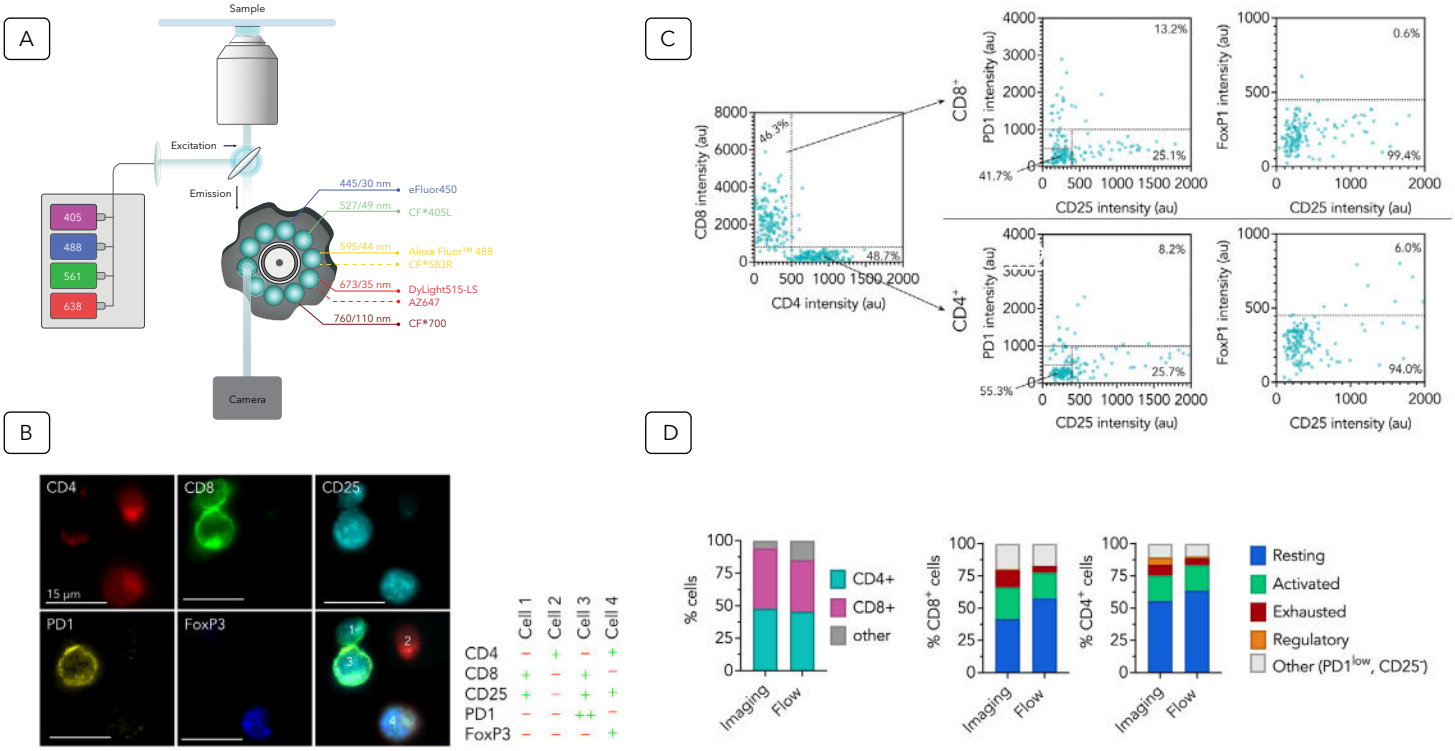

Figure 1 | Imaging multiple channels using Aplo Scope facilitates marker-based population classification.
A) Technical setup of Aplo Scope lasers and filters, and relevant combinations for the dyes used here (see also the methods section). B) Example region of PLL-captured T cells exhibiting differing cell marker classifications. Positivity is expressed with respect to isotype control samples. C) Intensity values for 326 individual T cells measured on Aplo Scope in 5 channels and their relevant gating into distinct subpopulations. Dotted lines indicate gating thresholds. D) Comparison of T cell subpopulation frequencies as reported by imaging and flow cytometry.

We then combined the cell-classification method with SMLM imaging, by capturing cells on a biologically relevant substrate as PLL might interfere with surface receptor nanoscale organization. A supported lipid bilayer (SLB) system was used in which an artificial fluid bilayer was deposited onto glass and loaded with relevant proteins to represent a minimal activatory setup: anti-CD3ε-Fab acting in place of cognate peptide-MHC to trigger the T cell receptor (TCR) in a clone-agnostic manner, and ICAM1 that acts as an adhesion ligand for LFA1 (Figure 2A). T cells were allowed to settle for 7 minutes before fixation, staining, and imaging. The same 5-color panel as above was used, with two additional targets for dSTORM imaging, the TCR with AZDye 647 and pZAP70 with CF®583R. Upon T-cell activation, the TCR intracellular signalling domains become phosphorylated and recruit ZAP70[14], which in turn becomes phosphorylated (pZAP70), and is able to drive downstream activatory signalling. During this process, TCR nano- and micro-clusters form to stabilize local kinase-enriched domains, constituting functional T cell activation units[15].

Consequently, reporting the nanoscale organization and relative distribution of TCR and pZAP70 is an informative readout on the status and nature of T cell activation. Staining in all five diffraction-limited channels allowed classification of individual cells into discrete subpopulations (Figure 2B), with an immediate functional readout being the frequency of T cell populations on the SLB surface compared to PLL, independently of super-resolution. Since the strong adhesion between LFA1 and ICAM1 is dependent on TCR-driven signalling[16], non-activated cells are likely not retained. Enrichments or depletions of a given population can inform its potential responsiveness to an phosphorylated (pZAP70), and is able to drive downstream activatory signalling. During this process, TCR nano- and micro-clusters form to stabilize local kinase-enriched functional readout being the frequency of T cell populations on the SLB surface compared to PLL, independently of super-resolution. Since the strong adhesion between LFA1 and ICAM1 is dependent on TCR-driven signalling[16], non-activated cells are likely not retained. Enrichments or depletions of a given population can inform its potential responsiveness to an activating substrate. In this case, the $CD4^+/CD8^+$ ratio was largely unaffected, whereas on the SLB the activated population was significantly enriched, and resting and exhausted populations depleted (Figure 2C). This is consistent with the known behavior of activated T cells, which have a lower subsequent activation threshold[17].

To quantitatively assess differences in nanoscale behavior between populations, TCR-derived localizations were grouped into discrete clusters using the DBSCAN function of ONI's CODI platform. Quantitative parameters for each cluster were derived and assigned to a given cell, previously assigned to a population as per the classification data (Figure 2D). There was no clear variability in TCR cluster metrics relating to cluster size, density, or number of TCR localizations per cluster between different T cell populations. To quantify pZAP70 association with TCR clusters, CODI's counting tool was used, in which the number of localizations in each channel was reported within a 100 nm radius of each cluster, approximately double the median TCR cluster radius (48.1 nm) (Figure 2E). The activated populations (both $CD4^+$ and $CD8^+$) exhibited significantly more pZAP70 localizations per TCR cluster than any other population, with median values of 35 ($CD4^+$) and 18 ($CD8^+$) pZAP70/cluster, compared to medians of ~10 for all other populations. This is evident in the ratio of pZAP70 localizations to TCR localizations within each cluster, which was larger in both activated populations than in any other. This is overall consistent with the known behavior of previously activated T cells being more responsive to TCR triggering than other T cell populations.

A

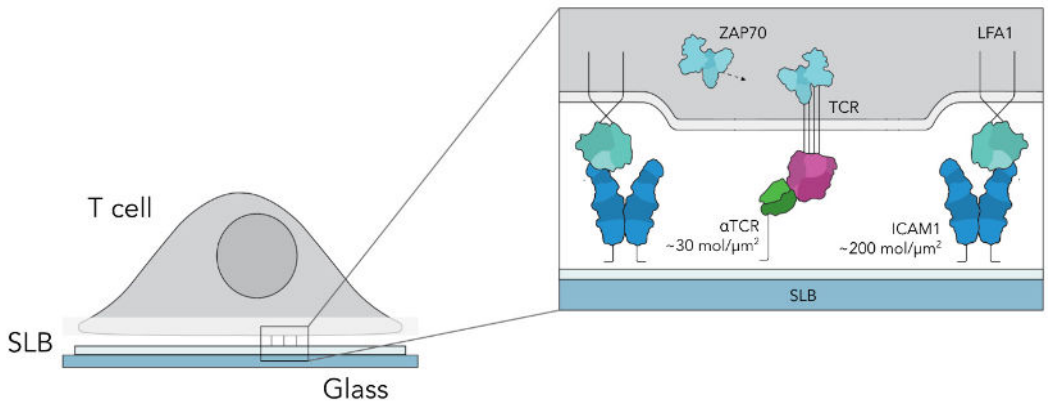

B

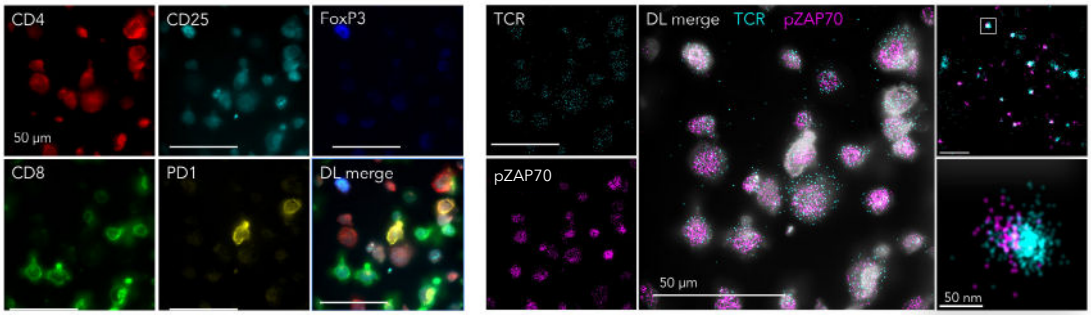

C

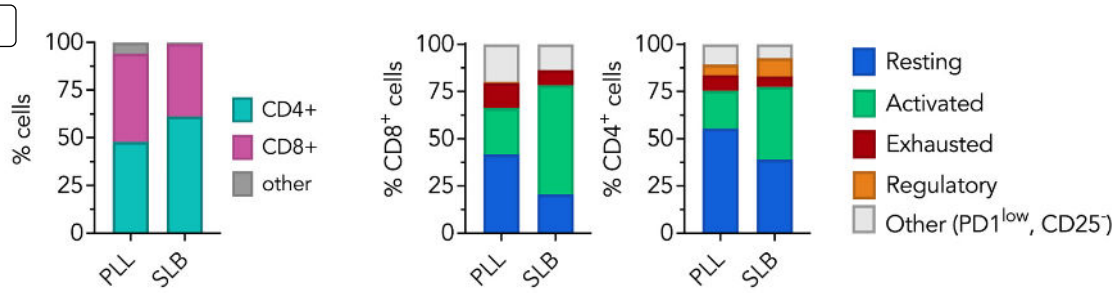

D

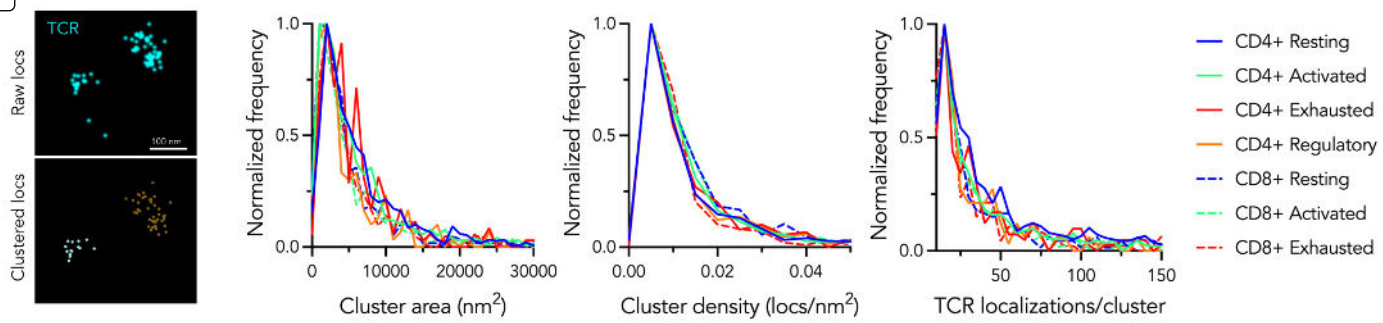

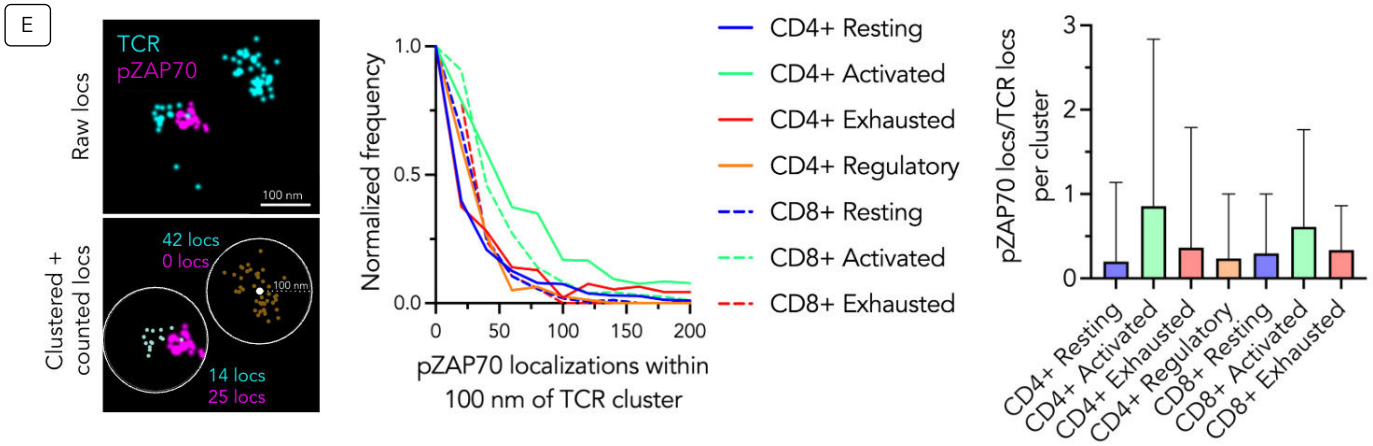

Figure 2 | Nanoscale dSTORM data can be mapped into marker-derived cell classifications.
A) Schematic representation of the SLB setup used and the key proteins involved. B) Example field-of-view of the 5 diffraction-limited ('DL', left) and 2 dSTORM (right) channels acquired on Aplo Scope. Zoomed regions correspond to boxes in larger images. C) Comparison of reported T cell subpopulation frequencies on PLL and SLB surfaces. PLL n = 326 cells, SLB n = 268 cells. D) Example of clustering process used in CODI (left) and histograms of output values for TCR cluster size, density, and TCR localization abundance across all T cell populations (right). E) Example of radial counting process used in CODI (left), histogram pZAP70 locs/cluster across populations (center), and graph showing the median + interquartile range of pZAP70 locs/TCR locs per cluster (right).

The ability to quantitatively assess cell activation with fine detail opens the potential to investigate the impact of positive and negative effectors on receptor behavior. Here, the impact of inhibitory signaling by PD1 was assessed by modifying the activating SLB to include PD1 ligand (PDL1) (Figure 3A). Upon PDL1 ligation, PD1 recruits inhibitory phosphatases such as SHP1/2, which dampen the activity of effectors such as TCR and CD28[18]. Looking at the population distribution on the PDL1-bearing SLB, the $CD4^+/CD8^+$ ratio was unchanged compared to the PDL1-negative SLB, however, the total fraction of retained activated and exhausted cells was reduced in both populations, while the fraction of resting cells increased (Figure 3B). This most likely reflects the fact that activated cells express PD1 (and exhausted cells have high PD1) and, thus, are more sensitive to inhibition of activation than the PD1- resting cells. The size of TCR clusters and the number of TCR localizations per cluster were somewhat reduced by the presence of PDL1, however, this was a modest effect and not strongly consistent across equivalent populations. In the case of cluster size this was significantly reduced in all activated and exhausted populations (Figure 3C). The largest impact of PDL1 was seen on associated pZAP70 localizations, which were greatly reduced in the activated and exhausted populations, but much less in resting cells (Figure 3D). Indeed, the distribution of pZAP70 localizations per cluster for the activated populations on the PDL1-bearing SLB was similar to that of the resting populations on the PDL1-negative SLB (Figure 3D, middle vs right).

A

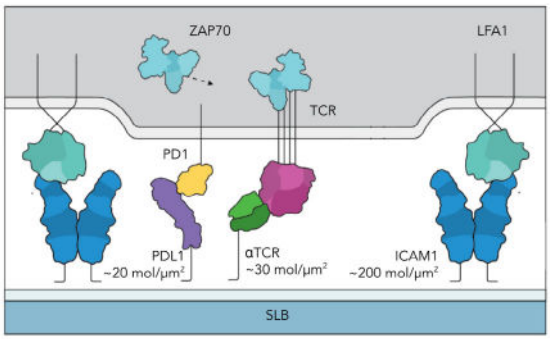

B

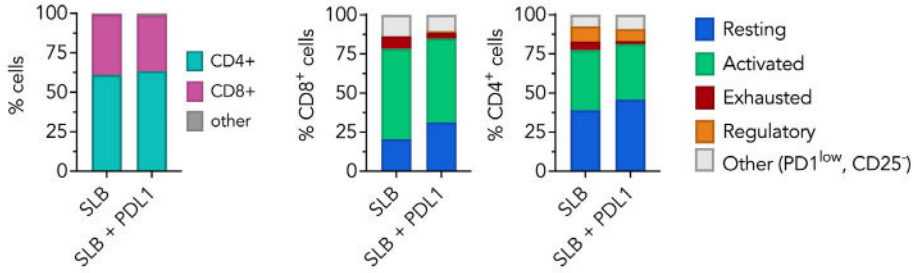

C

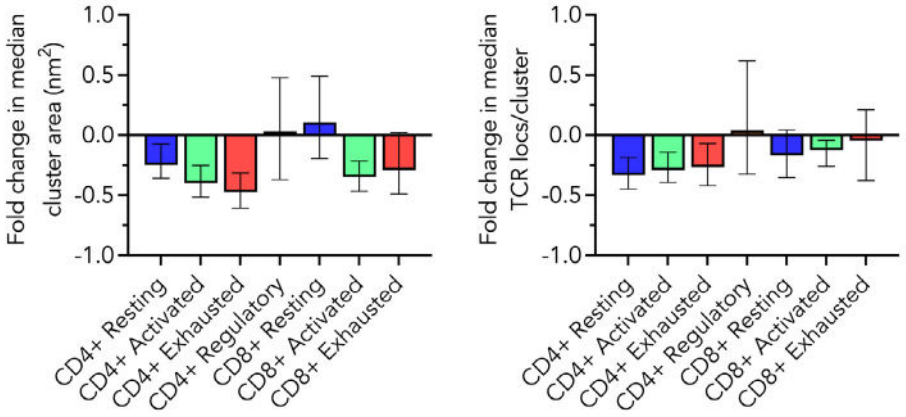

D

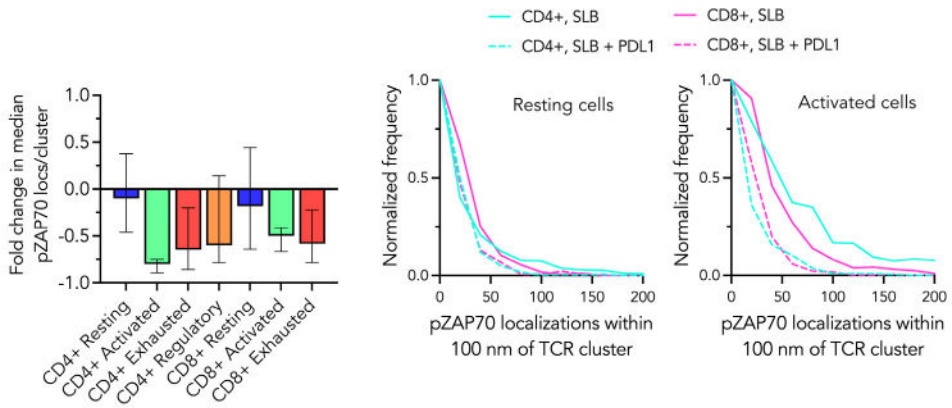

Figure 3 | dSTORM reports population-specific impacts of T cell co-inhibition.
A) Schematic representation of the PDL1-containing SLB setup. B) Comparison of reported T cell subpopulation frequencies on SLB surfaces with and without PDL1. SLB n = 268 cells, SLB + PDL1 n = 244 cells. C) Fold change in median TCR cluster area (left) and TCR locs/cluster (right) across populations in the presence of PDL1. Bars are median ± 95% confidence limits. D) Fold change in median pZAP70 locs/cluster (left) in the presence of PDL1, and histograms of pZAP70 locs/cluster for resting and activated populations on both SLB substrates (right).

SOLUTION WITH APLO SCOPE

In this study, the ability of Aplo Scope to provide high-quality multi-maker cell-characterization and single-molecule characterization data simultaneously in the same sample has been demonstrated. The combination of Aplo Scope with the Discovery Kit™: dSTORM in cells for sample preparation and CODI for data analysis yielded data that permitted the classification of a heterogeneous T cell sample into seven functional subpopulations, and the comparison of nanoscale receptor behavior between different subpopulations under activatory conditions. The observations detailed here are consistent with known T cell biology, however, they reflect the intricacy of detail that can be obtained through the powerful combination of cell characterization and dSTORM. Reporting nanoscale differences between subpopulations opens the door to a fuller understanding of the functional and behavioral differences between heterogeneous cells, which is in turn essential for the understanding of disease and the development of improved therapeutic interventions.

REFERENCES

1. Iyer RS et al. Drug-resistant EGFR mutations promote lung cancer by stabilizing interfaces in ligand-free kinase-active EGFR oligomers. Nat Comm. 2024; 15(213)
2. Bálint S et al. Supramolecular attack particles are autonomous killing entities released from cytotoxic T cells. Science 2020; 368(6493)
3. Wu H et al. Coronin 2B deficiency induces nucleolar stress and neuronal apoptosis. Cell Death Dis. 2024; 15(457)
4. Lelek M et al. Single-molecule localization microscopy. Nat Rev Methods Primers 2021; 1(39)
5. Jensen E & Crossman DJ. Technical review: types of imaging-direct STORM. Anat Rec 2014; 297(12)
6. Ando S and Araki K. CD8 T-cell heterogeneity during T-cell exhaustion and PD-1-targeted immunotherapy. Int Immunol. 2022; 34(11)
7. Wolmarans E et al. Heterogeneity of cell therapy products. S Afr Med J. 2019; 109(8b)
8. Ren Z et al. Cell Heterogeneity and Variability in Peripheral Nerve after Injury. Int J Mol Sci. 2024; 25(6)
9. Kumar BV et al. Human T cell development, localization, and function throughout life. Immunity. 2018; 48(2)
10. McKinnon K. Flow Cytometry: An Overview. Curr Protoc Immunol. 2018; 120(5)
11. Hwang B et al. Single-cell RNA sequencing technologies and bioinformatics pipelines. Exp Mol Med. 2018; 50
12. Labib M, Kelley SO. Single-cell analysis targeting the proteome. Nat Rev Chem. 2020; 4
13. Pasquale C. Image Cytometry: Protocols for 2D and 3D Quantification in Microscopic Images. Prog Hist Cyto. 2013; 47(4)
14. Germain RN. T-cell signaling: The importance of receptor clustering. Curr Biol. 1997; 7(10)
15. Dustin ML et al. Understanding the Structure and Function of the Immunological Synapse. Cold Spring Harb Perspect Biol. 2010; 2(10)
16. Hogg N et al. The insider's guide to leukocyte integrin signalling and function. Nat Rev Immunol 2011; 11
17. Viola A and Lanzavecchia A. T cell activation determined by T cell receptor number and tunable thresholds. Science. 1996; 273(5271)
18. Patsoukis N et al. Interaction of SHP-2 SH2 domains with PD-1 ITSM induces PD-1 dimerization and SHP-2 activation. Comm Biol. 2020; 3

